# Adaptation of Antarctic Icefish Vision to Extreme Environments

Gianni M. Castiglione (ORCID),*,[†,1,2,3,4,5] Frances E. Hauser,[1,6] Alexander Van Nynatten,[2,6] and Belinda S.W. Chang*,[1,2]

[1]Department of Ecology and Evolutionary Biology, University of Toronto, Toronto, ON, Canada

[2]Department of Cell and Systems Biology, University of Toronto, Toronto, ON, Canada

[3]Department of Biological Sciences, Vanderbilt University, Nashville, TN

[4]Department of Ophthalmology and Visual Sciences, Vanderbilt University Medical Center, Nashville, TN

[5]Evolutionary Studies, Vanderbilt University, Nashville, TN

[6]Department of Biological Sciences, University of Toronto Scarborough, Toronto, ON, Canada

[†]Present address: Department of Biological Sciences, Vanderbilt University, Nashville, TN.

*Corresponding authors: E-mails: belinda.chang@utoronto.ca; gianni.castiglione@vanderbilt.edu.

Associate editor: Guang Yang

## Abstract

**Extreme environments, such as Antarctic habitats, present major challenges for many biological processes. Antarctic icefishes (Crynotothenioidea) represent a compelling system to investigate the molecular basis of adaptation to cold temperatures. Here, we explore how the sub-zero habitats of Antarctic icefishes have impacted rhodopsin (RH1) function, the temperature-sensitive dim-light visual pigment found in rod photoreceptors. Using likelihood models and ancestral reconstruction, we find that accelerated evolutionary rates in icefish RH1 underlie unique amino acid mutations absent from other deep-dwelling fishes, introduced before (S160A) and during (V259M) the onset of modern polar conditions. Functional assays reveal that these mutations red-shift rhodopsin spectral absorbance, consistent with spectral irradiance under sea ice. These mutations also lower the activation energy associated with retinal release of the light-activated RH1, and accelerate its return to the dark state, likely compensating for a cold-induced decrease in kinetic rates. These are adaptations in key properties of rhodopsin that mediate rod sensitivity and visual performance in the cold dark seas of the Antarctic.**

*Key words:* **vision, icefish, rhodopsin.**

## Introduction

The Antarctic icefishes (Notothenioids) have a remarkable evolutionary history, originating from shallow marine environments off the coast of South America ~65 Ma, to now dominating 95% of biomass surrounding the Antarctic continent across a broad depth spectrum (0–3,000 m) uncommon in other deep-sea fauna assemblages (Near et al. 2015; Eastman 2017). With modern temperatures near the freezing point of saltwater (−1.9 °C), this adaptive radiation was facilitated by the evolution of antifreeze glycoproteins (AFGPs) to prevent intracellular ice formation (Cheng and Chen 1999). Accompanying a period of global cooling during the Oligocene, the evolution of AFGPs is thought to have triggered increased rates of lineage and phenotypic diversification in the Antarctic clade of Notothenioids (Cryonotothenioidea; hereafter referred to as "icefishes"; Eastman 2017), whereas other fauna were extirpated, providing novel ecological opportunities in this group (Matschiner et al. 2011; Near et al. 2012; Colombo et al. 2015). Following the origin of AFGPs, cryonotothenioids experienced major ecological niche diversification, associated with increases in species richness (Rutschmann et al. 2011; Near et al. 2012; Colombo et al. 2015; Eastman 2017). For example, in the most species-rich Cryonotothenioid clades, the crocodile icefishes (Channichthyidae), and Antarctic plunderfishes (Artedidraconidae), most contemporary diversity originated after the evolution of AFGP and coincides with the onset of modern polar conditions and increased ice activity during the late Miocene (Near et al. 2012; Colombo et al. 2015). The dynamic growth and retreat of the Antarctic ice sheet since then has likely driven Cryonotothenioids into deeper waters and also generating ecological opportunities for speciation (Janko et al. 2007; Barnes and Souster 2011; Kasparova et al. 2015; Barnes et al. 2016). Climate-induced changes to temperature and depth of these extreme habitats were therefore instrumental in shaping the Cryonotothenioidea radiation.

In addition to AFGPs, a suite of striking temperature-related gains and losses of gene and protein functions have been identified in Cryonotothenioidea (Kim et al. 2019),

**Open Access**

such as the loss of an inducible heat shock response (Hofmann et al. 2000, 2005), as well as the loss of hemoglobin expression in the crocodile icefishes (Ruud 1954; Cocca et al. 1995). Furthermore, multiple physiological pathways appear to have been optimized for cold temperatures through extensive modification of metabolic networks—a process which differs across Cryonotothenioidea depending on life history (Crockett and Sidell 1990; Kawall et al. 2002; Magnoni et al. 2013). Although cold adaptation in individual protein function is achieved by alterations to stability and binding strength (Siddiqui and Cavicchioli 2006; Fields et al. 2015; Peck 2016), the details of these changes can vary across Cryonotothenioidea proteins: Crocodile icefish (*Chionodraco hamatus*) peptide transporters achieve cold adaptation through increased ligand binding strength, whereas structural proteins such as eye lens crystallins have evolved in the Antarctic toothfish (*Dissostichus mawsoni*) to decrease binding strength in order to increase stability (Kiss et al. 2004; Rizzello et al. 2013). In contrast, Cryonotothenioidea enzymes display weakened substrate-binding and accelerated catalytic rates relative to warm-adapted species, likely a response to cold-induced decreases in kinetic rates (Beers and Jayasundara 2015). It has also been found that mutations in icefish lactate dehydrogenase $A_4$ ($A_4$-LDH) enzymes compensate for cold-induced decreases in kinetic rates by increasing flexibility of regions involved in conformational changes, thus reducing activation energy and increasing catalytic rates, but decreasing ligand binding through increased conformational entropy (Fields and Somero 1998; Fields et al. 2015). A key gap in our understanding of evolution to extreme cold is nonenzyme signaling proteins. These proteins face critical challenges in response to cold temperatures, as they depend on both conformational stability and ligand binding affinity to drive signaling function.

Rhodopsin, the temperature-sensitive dim-light visual pigment found in rod photoreceptors, is of special importance to deep-diving fishes such as the Cryonotothenioidea and presents an excellent opportunity to investigate the evolution of an important sensory protein in response to extreme conditions (Hunt et al. 2001; Sugawara et al. 2010; Castiglione et al. 2017, 2018). Natural variation in rhodopsin is often associated with spectral tuning to the photic environment in the form of shifts in the pigments' wavelength of maximal absorbance ($\lambda_{MAX}$), wherein light detection is enhanced in deep-diving organisms through spectral tuning mutations that blue shift the wavelength of maximum absorbance to match the composition of downwelling light (Yokoyama et al. 1999; Hunt et al. 2001; Van Nynatten et al. 2015; Dungan et al. 2016; Hauser and Chang 2017). Light is rapidly attenuated in marine environments and eventually results in complete darkness at depths >1,000 m (Denton 1990). This attenuation is further enhanced in Antarctic waters covered by snow and thick sea ice, limiting dim-light vision to a maximum depth around 30–60 m, where Cryonotothenioid rod sensitivities peak among 500 nm, matching red-shifted spectral irradiance under ice (Sullivan et al. 1983; Buckley and Trodahl 1987; Pankhurst and Montgomery 1989; Morita et al. 1997; Pointer et al. 2005).

Rhodopsin detects photons through isomerization of its chromophore 11-*cis* retinal (11CR) to all-*trans* retinal, causing a series of temperature-sensitive conformational changes that result in equilibria among active-state rhodopsin intermediates (Schafer et al. 2016; Van Eps et al. 2017), of which the active (MII) state is capable of activating G protein transducin ($G_t$) (Kojima et al. 2014), ultimately resulting in a neural signal (Ebrey and Koutalos 2001). Interestingly, although increasing rod: cone ratios and elongated rod outer segments likely confer increased photosensitivity in some deep-dwelling Cryonotothenioids (*D. mawsoni*), the retina of other Cryonotothenioid species (*Pagothenia borchgrevinki*) appear highly photosensitive, despite displaying no obvious anatomical adaptations that would indicate enhanced dim-light sensitivity (Meyer-Rochow and Klyne 1982; Eastman 1988; Morita et al. 1997; Pointer et al. 2005). Cold temperatures may be convenient way to enhance photosensitivity via decreased spontaneous thermal activation of rhodopsin (Aho et al. 1988); however, these extreme conditions likely place substantial barriers on the rate of dark adaptation and regeneration of photosensitivity in Antarctic poikilotherm fauna (Meyer-Rochow 1982; Meyer-Rochow and Fleming 1997). Recent evidence suggests that the decay rates of light-activated rhodopsin (MII) are indeed impacted by colder temperatures, where high-altitude Andean and Himalayan specialist catfishes each possess rare amino acid substitutions accelerating MII decay, likely compensating for cold-induced decreases in these physiologically important kinetic rates associated with regeneration of photosensitivity (Castiglione et al. 2017, 2018). It is not known if rhodopsin from extremophile Antarctic icefishes also exhibits adaptation in kinetic rates, and if these may be achieved through similar molecular mechanisms.

To examine the combined effects of both temperature and light environment on icefish visual pigments, we investigated whether icefish rhodopsins display accelerated evolution relative to nonicefish outgroups and tested for functional properties consistent with cold adaptation. We also investigated whether spectral tuning mutations are present, given the effects of ice and habitat depth on downwelling irradiance. How does spectral adaptation to depth intersect with functional adaptation to cold to produce novel protein phenotypes? We implement a combination of molecular evolutionary analyses, structural modeling, and protein assays to address these questions. We find evidence of positive selection at amino acid sites with rare rhodopsin variants that, when assayed experimentally using in vitro model systems, accelerate kinetic rates and decrease activation energy required for return of the dark-state conformation. One of these mutations also red-shifted rhodopsin spectral absorbance, suggesting adaptation to red-shifted light spectra under sea ice (Sullivan et al. 1983;

Buckley and Trodahl 1987; Pankhurst and Montgomery 1989). Our results suggest that rhodopsin can adapt to light and temperature simultaneously.

## Results

### Positive Selection on Rhodopsin Accompanied Periods of Rapid Icefish Diversification Associated With Ancient Climate Change

Relative to warm-dwelling outgroups, we hypothesized that Antarctic icefishes (Crynotothenioidea) would display accelerated rhodopsin evolutionary rates, potentially reflecting rhodopsin functional adaptation. To test this, we first constructed a large icefish rhodopsin coding sequence data set ($n = 74$). Since there are multiple conflicting icefish phylogenies (Parker et al. 2021), we took a conservative approach and estimated an RH1 gene tree for use in our dN/dS analyses (see Methods). We found significant evidence of positive selection across the notothenioids (tables 1 and 2), as well as within the

AFGP-containing Cryonotothenioidea (table 3). We next explicitly investigated clade- and lineage-specific differences in evolutionary rates using Clade model C (CmC) (Bielawski and Yang 2004). Since icefishes experienced two major climate-linked episodes of accelerated diversification: (1) immediately after the origin of AFGP and the Cryonotothenioid suborder; (2) more recently during the onset of modern polar conditions, we investigated evidence of accelerated evolution at both nodes, which are phylogenetically nested (fig. 1A–C). We found evidence of accelerated evolutionary rates in the Cryonotothenioid clade, which includes all AFGP-containing Notothenioids (fig. 1D; table 4). Furthermore, we found a significant acceleration in evolutionary rates between Noto- and Cryonotothenioids (fig. 1D; table 4). This suggests that the molecular evolutionary rates of rhodopsin accelerated during the diversification of the Cryonothenioidea after the AFGP innovation. Relative to all other cryonothenioids, we found evidence of shifts in evolutionary rates on the two most species rich and recently diversifying lineages: epipelagic crocodile icefishes lacking

**Table 1.** Analyses of Selection on Notothenioid and Outgroup Rhodopsin (rh1) Using PAML Random Sites Models.

| Model | ln L | Parameters[a] | | | Null | P-value [df][b] | Δ AIC[c] |
|---|---|---|---|---|---|---|---|
| | | $\omega_0/p$ | $\omega_1/q$ | $\omega_2/\omega_p$ | | | |
| M0 | −5,549.19 | 0.36 | – | – | N/A | – | 969.32 |
| M1a | −5,176.90 | 0.02 (77%) | 1.00 (23%) | – | M0 | 0.000 [1] | 226.75 |
| M2a | −5,066.39 | 0.02 (74%) | 1.00 (22%) | 6.86 (3%) | M1a | 0.000 [2] | 9.72 |
| M3 | −5,066.09 | 0.02 (75%) | 1.10 (22%) | 7.58 (3%) | M0 | 0.000 [4] | 11.12 |
| M7 | −5,161.48 | 0.07 | 0.25 | – | N/A | – | 195.9 |
| M8a | −5,155.87 | 0.13 | 2.13 | 1.00 | N/A | – | 186.7 |
| M8 | −5,061.53 | 0.06 | 0.22 | 6.40 | M7 | 0.000 [2] | 0* |
| | | | | | M8a | 0.000 [1] | |

[a]$\omega$ values of each site class are shown are shown for models M0–M3 ($\omega_0$–$\omega_2$) with the proportion of each site class in parentheses. For M7 and M8, the shape parameters, $p$ and $q$, which describe the beta distribution are listed instead. In addition, the $\omega$ value for the positively selected site class ($\omega_p$, with the proportion of sites in parentheses) is shown for M8.
[b]Significant P-values ($\alpha \le 0.05$) are bolded. Degrees of freedom are given in square brackets after the P-values.
[c]Model fits were assessed by Akaike information criterion differences to the best-fitting model (bolded asterisk).
lnL, ln Likelihood; N/A, not applicable.

**Table 2.** Analyses of Selection on Notothenioid Rhodopsin (rh1) Using PAML Random Sites Models.

| Model | lnL | Parameters[a] | | | Null | P-value [df][b] | Δ AIC[c] |
|---|---|---|---|---|---|---|---|
| | | $\omega_0/P$ | $\omega_1/q$ | $\omega_2/\omega_p$ | | | |
| M0 | −4,124.72 | 0.48 | – | – | N/A | – | 740.97 |
| M1a | −3,859.73 | 0.03 (79%) | 1.00 (21%) | – | M0 | 0.000 [1] | 212.99 |
| M2a | −3,758.97 | 0.02 (75%) | 1.00 (20%) | 7.42 (5%) | M1a | 0.000 [2] | 15.47 |
| M3 | −3,750.23 | 0.06 (82%) | 1.94 (15%) | 12.22 (3%) | M0 | 0.000 [4] | 0* |
| M7 | −3,862.69 | 0.01 | 0.02 | – | N/A | – | 218.92 |
| M8a | −3,855.82 | 0.17 | 3.70 | 1.00 | N/A | – | 207.17 |
| M8 | −3,759.21 | 0.02 | 0.05 | 7.38 | M7 | 0.000 [2] | 15.94 |
| | | | | | M8a | 0.000 [1] | |

[a]$\omega$ values of each site class are shown are shown for models M0–M3 ($\omega_0$–$\omega_2$) with the proportion of each site class in parentheses. For M7 and M8, the shape parameters, $p$ and $q$, which describe the beta distribution are listed instead. In addition, the $\omega$ value for the positively selected site class ($\omega_p$, with the proportion of sites in parentheses) is shown for M8.
[b]Significant P-values ($\alpha \le 0.05$) are bolded. Degrees of freedom are given in square brackets after the P-values.
[c]Model fits were assessed by Akaike information criterion differences to the best-fitting model (bolded asterisk).
lnL, ln Likelihood; N/A, not applicable.

**Table 3.** Analyses of Selection on Cryonotothenioid Rhodopsin (*rh1*) Using PAML Random Sites Models.

| Model | lnL | Parameters[a] | | | Null | P [df][b] | Δ AIC[c] |
|---|---|---|---|---|---|---|---|
| | | $\omega_0/p$ | $\omega_1/q$ | $\omega_2/\omega_p$ | | | |
| M0 | −3,329.86 | 0.62 | – | – | N/A | – | 634.11 |
| M1a | −3,123.59 | 0.02 (81%) | 1.00 (19%) | – | M0 | 0.000 [1] | 223.57 |
| M2a | −3,027.60 | 0.02 (77%) | 1.00 (17%) | 7.67 (6%) | M1a | 0.000 [2] | 35.58 |
| M3 | −3,008.81 | 0.06 (84%) | 2.76 (13%) | 13.7 (3%) | M0 | 0.000 [4] | 0* |
| M7 | −3,129.34 | 0.012 | 0.024 | – | N/A | – | 235.07 |
| M8a | −3,129.31 | 0.34 | 15.9 | 1.00 | N/A | – | 237.00 |
| M8 | −3,022.56 | 0.010 | 0.032 | 7.90 | M7 | 0.000 [2] | 25.51 |
| | | | | | M8a | 0.000 [1] | |

[a]$\omega$ values of each site class are shown are shown for models M0–M3 ($\omega_0$–$\omega_2$) with the proportion of each site class in parentheses. For M7 and M8, the shape parameters, $p$ and $q$, which describe the beta distribution are listed instead. In addition, the $\omega$ value for the positively selected site class ($\omega_p$, with the proportion of sites in parentheses) is shown for M8.
[b]Significant $P$-values ($\alpha \leq 0.05$) are bolded. Degrees of freedom are given in square brackets after the $P$-values.
[c]Model fits were assessed by Akaike information criterion differences to the best-fitting model (bolded asterisk).
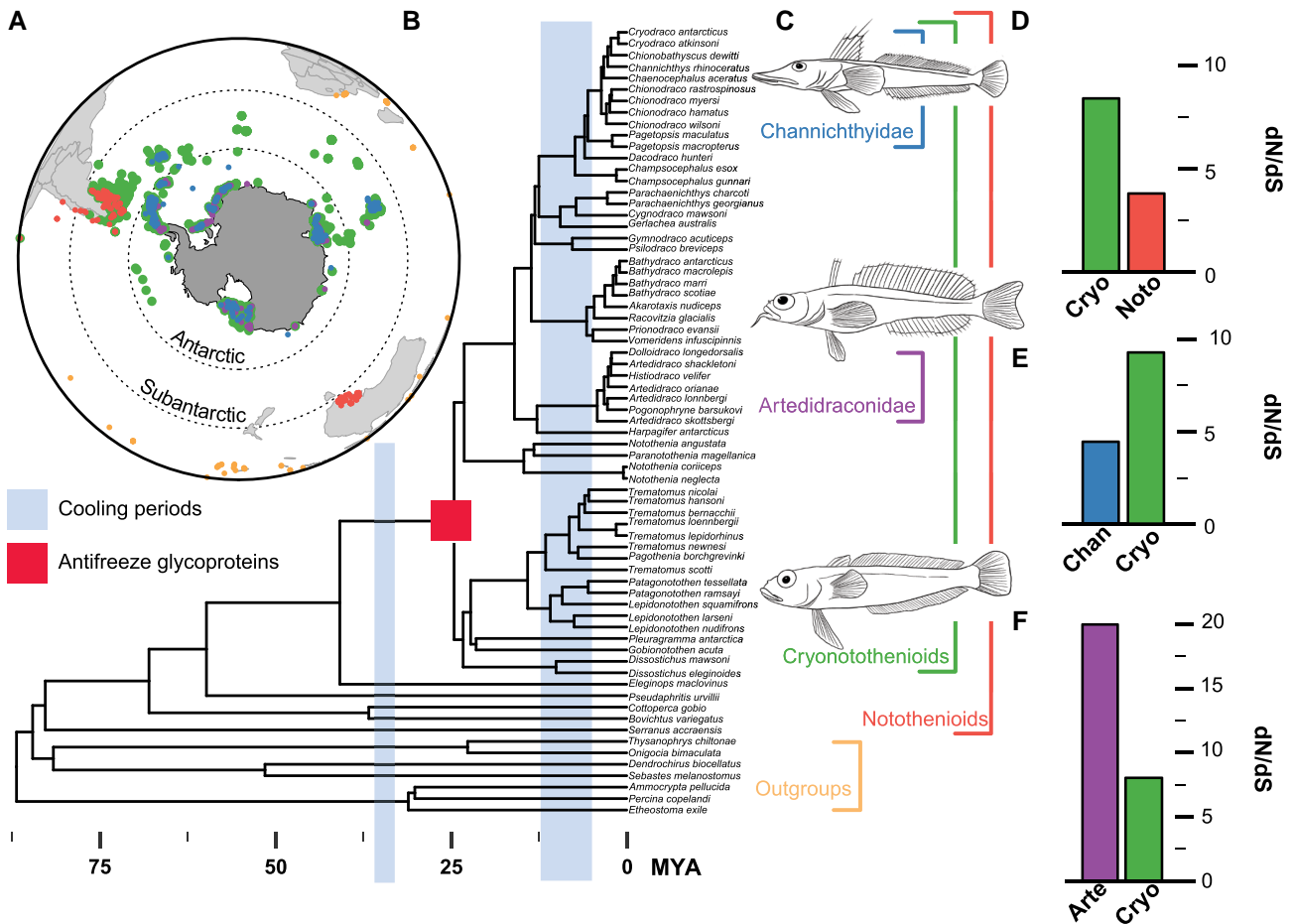lnL, ln Likelihood; N/A, not applicable.



**FIG. 1.** Accelerated evolutionary rates in icefish rhodopsin. (A) Geographic distribution of icefishes and outgroup species collected from the Global Biodiversity Information Facility. All catch data for each species are displayed and colored according to the classifications in (B). (B) Phylogenetic relationships of icefishes and outgroups from Rabosky et al. (2018). Periods of cooling (blue) before and after the evolution of AFGPs (red) are shown according to Near et al. (2012). (C) Rhodopsin (*rh1*) evolutionary rates of: (D) Notothenioids relative to all Antarctic cyronotothenioids; (E) Channichthyidae relative to other cyronotothenioids; and (F) Artedidraconidae relative to other cyronotothenioids.

hemoglobin (Channichytidae), where evolutionary rates are more conserved; and the demersal Antarctic plunderfishes (Artedraconidae), where evolutionary rates have accelerated (fig. 1E and F; table 4). These signatures of selection suggest icefish RH1 has functionally adapted across different icefish lineages.

**Table 4.** Results of Clade Model C (CmC) Analyses of Notothenioid *rh1* Under Various Partitions.

| Model and Foreground[a] | ΔAIC[d] | lnL | Parameters[b] | | | Null | P-value [df][c] |
|---|---|---|---|---|---|---|---|
| | | | $\omega_0$ | $\omega_1$ | $\omega_2/\omega_d$ | | |
| M2a_rel | 31.7 | −5,066.39 | 0.02 (74%) | 1 (22%) | 6.87 (3%) | N/A | – |
| CmC_*Noto* | 6.73 | −5,052.92 | 0.02 (74%) | 1 (21%) | 2.11 (5%) Noto: 7.46 | M2a_rel | **0.000 [1]** |
| CmC_*Cryo* | 2.29 | −5,050.72 | 0.02 (74%) | 1 (20%) | 2.58 (5%) Cryo: 8.50 | M2a_rel | **0.000 [1]** |
| **CmC_*Noto* versus *Cryo*** | 0.98 | −5,049.05 | 0.02 (74%) | 1 (21%) | 2.09 (5%) Noto: 3.85 Cryo:8.42 | M2a_rel | **0.000 [2]** |
| CmC_*Noto* versus *Cryo* w fixed[b] | 215.37 | −5,157.24 | 0.01 (74%) | 1 (19%) | 0.10 (8%) Noto: 0.00 Cryo: 1.00 | CmC_fix M2a_rel | **0.000 [1]** 1 [1] |
| **CmC_*Art*** | 24.80 | −5,031.96 | 0.02 (74%) | 1 (21%) | 5.03 (5%) Art: 21.9 | M2a_rel | **0.000 [1]** |
| **CmC_*Chann*** | 33.0 | −5,066.06 | 0.02 (74%) | 1 (22%) | 6.97 (3%) Chann: 5.09 | M2a_rel | **0.000 [1]** |
| **CmC_*Cryo* versus *Art*** | 0.08 | −5,048.60 | 0.02 (74%) | 1 (21%) | 2.66 (5%) Cryo: 8.03 Art: 20.5 | M2a_rel | **0.000 [2]** |
| CmC_*Cryo* versus *Art* w fixed[b] | 38.29 | −5,068.71 | 0.02 (74%) | 1 (21%) | 2.72 (5%) Cryo:8.07 Art:1.00 | CmC_fix M2a_rel | **0.000 [1]** 1 [1] |
| **CmC_*Cryo* versus *Chann*** | 0.00 | −5,048.56 | 0.02 (74%) | 1 (21%) | 2.57 (5%) Cryo: 9.26 Chann: 4.47 | M2a_rel CmC_fix | **0.000 [2]** **0.000 [1]** |
| CmC_*Cryo* versus *Chann* w fixed[b] | 13.29 | −5,056.20 | 0.02 (74%) | 1 (21%) | 2.55 (5%) Cryo: 9.22 Chann: 1.00 | M2a_rel | **0.000 [1]** |
| CmC_*Cryo* versus *Art/Chann* | 4.11 | −5,050.61 | 0.02 (74%) | 1 (21%) | 2.57 (5%) Cryo:8.70 Art/Chann:7.69 | M2a_rel | **0.000 [1]** |
| CmC_*Cryo* versus *Art* versus *Chann* | 9.66 | −5,052.39 | 0.02 (74%) | 1 (21%) | 2.59 (5%) Cryo:8.74 Art: 19.8 Chann: 4.47 | M2a_rel | **0.000 [1]** |

[a]The foreground partition is listed after the underscore for the clade models and consists of either: the clade of Notothenioid fishes (*Noto*); the clade Cryonotothenioids (*Cryo*); the clade artedidraconidae (*Art*); or the clade channichthyidae (*Chann*). These clades can also be set as two separate foregrounds (e.g., *Noto* vs. *Cryo*) or the same foreground (e.g., *Art/Chann*). In any partitioning scheme, the entire clade was tested, and all nonforeground data are present in the background partition.

[b]$\omega_d$ is the divergent site class, which has a separate value for the foreground and background partitions. "w fixed" indicates wd being set to 1.

[c]Significant *P*-values ($\alpha \leq 0.05$) are bolded. Degrees of freedom are given in square brackets after the *P*-values.

[d]All ΔAIC values are calculated from the lowest AIC model. The top two best fits are bolded with an asterisk (*).

lnL, ln Likelihood; AIC, Akaike information criterion.

## Positively Selected Sites Include Rare Variants at Key Locations in Rhodopsin Structure

To better understand the functional relevance of positively selected sites within Cryonotothenioidea (table 5), we cross-referenced icefish rhodopsin residues at these positions with a rhodopsin alignment representing a wide phylogenetic range of vertebrates (supplementary tables S1 and S2, Supplementary Material online). We found rare amino acid variants in icefish RH1 at positively selected sites 160 and 259 (A160; M259) that were absent in other vertebrates (fig. 2A). This suggests that the functional constraints on these sites present in vertebrate rhodopsin have shifted in icefish rhodopsins. To explore the relation of these mutations to climate and speciation events, we investigated substitution patterns across the Cryonotothenioid phylogeny using ancestral reconstruction. We found that the rare amino acid variants A160 and M259 were introduced near the

origin of the Cryonotothenioidea radiation (where AFGP evolved; fig. 2A) and Artedidraconidae clade, respectively, which together represent the two key periods of adaptation and speciation in response to climatic change events (Near et al. 2012; Colombo et al. 2015). This suggests that the introduction of these mutations is associated with icefish diversification that occurred alongside the onset of modern polar conditions.

In addition to these natural variants unique to icefish RH1, we also found the well-known spectral tuning mutation E122Q (Sakurai et al. 2007; Yokoyama et al. 2008) in several cryonotothenioid lineages, consistent with the deep-dwelling nature of several cryonotothenioid species (fig. 2A and B). However, this site is also an important determinant of active-state rhodopsin (MII) stability, which determines the rate of chromophore release (Imai et al. 2005; Castiglione and Chang 2018;

**Table 5.** Bayes Empirical Bayes Posterior Probabilities of Sites Under Selection. *Rh1* sites inferred to be under positive selection in the best fitting random sites models (M8) as well as that from the best-fitting CmC partitioning schemes.

| | M8 Cryonotothenioids | CmC_*Noto* versus *Cryo* | CmC_*Cryo* versus *Chann* | CmC_*Cryo* versus *Art* |
|---|---|---|---|---|
| 112 | 1 | 0.99998 | 0.99997 | 0.99997 |
| 122 | 0.931 | 0.58822 | 0.53792 | – |
| 133 | – | 0.72431 | 0.70966 | 0.67645 |
| 158 | 0.998 | 0.99926 | 0.99935 | 0.99924 |
| 160 | 0.776 | 0.93991 | 0.89991 | 0.89742 |
| 162 | 0.912 | 0.99638 | 0.99833 | 0.99817 |
| 165 | 1 | 1 | 1 | 1 |
| 166 | 0.608 | 0.60474 | 0.51177 | |
| 209 | 1 | 1 | 1 | 1 |
| 213 | 1 | 1 | 1 | 1 |
| 214 | 0.999 | 0.99448 | 0.98812 | 0.98457 |
| 216 | 0.999 | 0.99332 | 0.99074 | 0.99043 |
| 217 | 1.000 | 1 | 1 | 1 |
| 218 | 0.639 | 0.80523 | 0.78603 | 0.75418 |
| 256 | 0.586 | 0.82838 | 0.78337 | 0.75402 |
| 259 | 1 | 0.99859 | 0.99632 | 0.9962 |
| 263 | – | 0.72328 | 0.59327 | 0.55016 |
| 266 | 1 | 0.99998 | 0.99999 | 0.99999 |
| 270 | 0.994 | 0.97775 | 0.97632 | 0.97177 |
| 274 | – | 0.72768 | 0.89467 | 0.88614 |

Note.—Notothenioid fishes (*Noto*); Cryonotothenioids (*Cryo*); Artedidraconidae (*Art*); Channichthyidae (*Chann*).

Van Nynatten et al. 2021). Similarly, we also observed the D83N substitution across several cryonotothenioid lineages, which is another well-known spectral tuning mutation with pleiotropic effects on MII kinetics (Sugawara et al. 2010; Dungan and Chang 2017; Hauser et al. 2017). The presence of these two well-known mutations suggests that both spectral and nonspectral kinetic functions are modified in Antarctic icefish RH1. Unlike E122Q and D83N, which display a worldwide distribution among deep-dwelling fishes and whales (Sugawara et al. 2010; Dungan and Chang 2017; Hauser et al. 2017), the rare variant M259 is only observed to our knowledge at the origin of the speciose Antarctic plunderfishes (V259M; Artedraconidae). This mutation occurs within the important TM6 kink, which may affect the activation kinetics of this important domain (Choe et al. 2011; fig. 2C). Moreover, the rare variant T160A appears to be unique to the origin of the Cryonotothenioidea and is predicted to remove the hydrogen bonding ability of the R-group at site 160 (TM4), which may be required to stabilize the active conformation via interaction with N78 (TM2) that "sandwich" TM3 (i.e., site 122) in the active-helix conformation (fig. 2D; Choe et al. 2011). Based on this, it is possible that T160A will destabilize the MII active conformation, accelerating conformational decay to the dark state, which is required for dark adaptation after light bleaches (Palczewski et al. 2000; Ernst et al. 2014). The absence of these two mutations from other deep-dwelling fishes to our knowledge implies that an ecological variable unique to their extreme habitats may be driving the signatures of positive selection we detected in icefish rhodopsin. Taken together with their

structural locations, we hypothesized that the rare variants A160 and M259 may alter rhodopsin kinetic properties as an adaptation to cold temperatures.

## Icefish Mutations Significantly Alter the Spectral Sensitivity and Activation Kinetics of Rhodopsin

We conducted functional assays to test the effects of rare variants A160 and M259 on rhodopsin. First, we tested whether sites containing natural positively selected Antarctic variants (T160A and I259M) from crocodile icefishes (Channichthyidae) and Antarctic plunderfishes (Artedraconidae) could be under selection as a result of the red-shifted spectral content of water covered by a layer of ice (490–550 nm) (Sullivan et al. 1983; Buckley and Trodahl 1987; Pankhurst and Montgomery 1989). We tested this experimentally through in vitro expression and spectroscopic assays of rhodopsin function, which require high protein concentrations and have therefore been extensively optimized for use on the model bovine (*Bos taurus*) rhodopsin. Bovine rhodopsin is also represented by well-resolved crystal structures of both active and inactive states, allowing for robust interpretation of functional results (Palczewski et al. 2000; Choe et al. 2011). To further validate the suitability of bovine rhodopsin for testing the effects of rare natural variants from icefishes, we performed homology modeling of rhodopsin from icefish. To maintain focus on the protein background, we utilized an icefish RH1 that does not contain the rare variants at sites 160 and 259 (*C. hamatus*). In comparison with the active state (MII) of bovine rhodopsin, the predicted MII of icefish rhodopsin displays a nearly identical arrangement of transmembrane helices (supplementary fig. S3, Supplementary Material online). Moreover, the residues surrounding sites 160 and 259 are highly conserved between bovine and icefish rhodopsin and display overlapping orientations in the predicted structure (supplementary fig. S3, Supplementary Material online). Thus, unlike other species' rhodopsins where the sites of interest are immediately proximal to nonconserved sites (Dungan and Chang 2017), sites 160 and 259 display substantial conservation between icefish and bovine rhodopsin at both the sequence and structure levels. This strongly suggests that the potential for confounding background effects is minimal.

We therefore proceeded to perform site-directed mutagenesis to alter WT bovine residues to the rare natural variants in Channichthyidae and Artedraconidae. WT rhodopsin, along with T160A and I259M mutants, were expressed in HEK293T cells, regenerated with 11-*cis*-retinal, and immunoaffinity purified. All mutant RH1 proteins displayed comparable expression levels to WT (fig. 3A; A280). We measured the dark-state $\lambda_{MAX}$ of WT and mutant rhodopsins, finding that WT rhodopsin produced a $\lambda_{MAX}$ of 499 nm, similar to previously published results (fig. 3A; Guo et al. 2014; Van Eps et al. 2017). T160A produced a red shift to 502 nm, whereas I259M produced no spectral shift relative to WT (499 nm; fig. 3A; table 6).
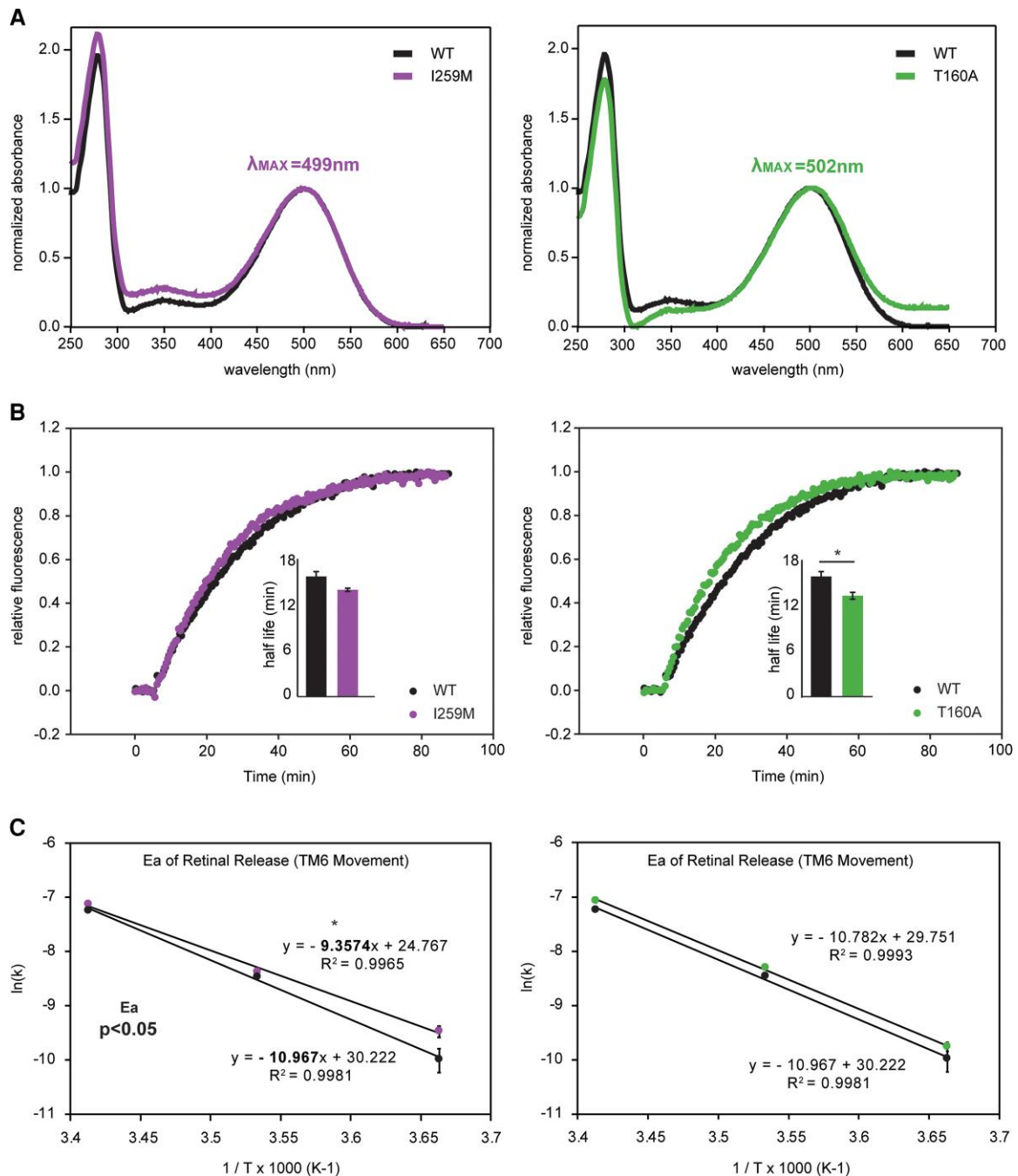
**Fig. 2.** Icefish rhodopsin amino acid substitutions occur in flexible structural regions governing protein stability and spectral tuning. (*A*) Phylogenetic distribution of icefish rhodopsin substitutions, which include novel variants at sites 160 and 259, as well as known spectral tuning mutations at sites 83 and 122. Branch lengths represent the number of amino acid substitutions per amino acid site, shown on the rh1 gene tree (Methods). (*B*) Rhodopsin dark-state structure (1U19) with sites of interest highlighted. Retinal chromophore is shown in black. (*C*) Site 259 is located on helix 6, which undergoes major conformational changes in response to light activation to the MII state (3PQR). (*D*) Site 160 stabilizes helix 3 in the light-activated confirmation.

We next examined the effects of these natural Antarctic variants (T160A and I259M) on the kinetics of rhodopsin, which are of direct relevance to organismal visual sensitivity and are known to adapt rhodopsin function to cold temperatures in other fishes (Aho et al. 1988; Castiglione et al. 2017; Castiglione et al. 2018). We found that T160A significantly accelerated the decay of light-activated rhodopsin (MII) relative to WT (fig. 3*B*; table 6), thus promoting a return to the rhodopsin dark state. Furthermore, we found that I259M significantly reduced the activation energy of MII decay (fig. 3*C*; tables 7–9), lowering the energy required for retinal release, ultimately allowing rhodopsin to return the dark state (Schafer and Farrens 2015; Van Eps et al. 2017). Reducing the activation energy also means that at the lower temperatures at which these fishes live, the rate of release is disproportionally higher, resulting in a more substantial rate difference when compared with WT rhodopsin (supplementary fig. S2, Supplementary Material online). Thus, both icefish rhodopsin mutations

contribute to adaptations that increase kinetic rates, and in the case of I259M, lower the kinetic barriers that prevent rhodopsin from returning to the dark-state conformation. Since dark-state rhodopsin is required for regaining dim-light vision after light exposure, these results strongly suggest that selection has introduced these mutations to compensate for a cold-induced decrease in RH1 kinetic rates.

## Discussion

Natural variation in enzyme proteins has revealed a rich array of adaptations in response to cold temperatures across cold-adapted organisms (Siddiqui and Cavicchioli 2006; Fields et al. 2015; Peck 2016). Signaling proteins such as rhodopsin are likely untapped sources of variation (relative to enzymes) for examining shifts in kinetic properties that compensate for temperature fluctuations. We used a combination of molecular evolutionary analyses and functional

**FIG. 3.** Icefish mutations produce spectral tuning and kinetic cold adaptation in rhodopsin. (A) Absorbance spectroscopy determining the spectral sensitivity ($\lambda_{MAX}$) of wild-type (WT) and bovine rhodopsin mutants containing residues unique to icefish rhodopsin (T160A or I259M). (B) Fluorescence spectroscopy of WT and mutant rhodopsins at 20 °C. Increasing fluorescence represents all-trans retinal release, which reflects the decay of the rhodopsin light-activated conformation (MII decay). Inset denotes the half-life values (minutes). (C) Arrhenius plots of WT and mutant rhodopsin retinal release rates ($k$). The slope of each regression represents the activation energy (Ea) of retinal release, and thus the decay of transmembrane helix (TM) 6 to the dark-state conformation (temperature as inverse kelvin ($K$); $T$ = degrees Celsius).

**Table 6.** Summary of Spectroscopic Assays on WT and Mutant Rhodopsins.

| Pigment | $\lambda_{MAX}$ (nm)[a,b] | Half-life of retinal release (minutes)[a,b] | | |
|---|---|---|---|---|
| | | 20 °C | 10 °C | 0 °C |
| WT bovine rhodopsin | 498.9 ± 0.05 (3) | 16.2 ± 0.7 (3) | 54.6 | 266.7 ± 70.9 (3) |
| T160A | 501.7 ± 1.4 (3) | 13.6 ± 0.5 (3) | 46.8 | 202.7 ± 29 (3) |
| I259M | 499 ± 0.1 (3) | 14.4 ± 0.2 (3) | 50.2 | 151.3 ± 14 (3) |

[a]Standard error is shown.
[b]Number of biological replicates (i.e., separate elutions and/or purifications of rhodopsin) is shown in brackets.

protein assays to investigate novel adaptations to cold temperatures in icefish rhodopsin. We found accelerated evolutionary rates in rhodopsin in rapidly radiating extremophile icefish. Next, we identified novel amino acid substitutions under positive selection in these specialist fishes that do not occur elsewhere in vertebrate rhodopsin proteins. These mutations, when introduced into rhodopsin and functionally assayed, were found to significantly shift both its spectral and kinetic properties, likely tuning the protein to optimize its function at cold temperatures. Here, we discuss our results in the context of cold adaptation in extreme environments, and functional convergence in rhodopsin proteins.

## Naturally Occurring Mutations Drive Cold Adaptation of Icefish Rhodopsin

Protein activation kinetics have been extensively tuned to optimize function in variable, and often extreme, environments. Kinetic rates increase in cold-adapted enzymes (Siddiqui and Cavicchioli 2006; Fields et al. 2015; Peck 2016). For example, in icefish enzymes, key mutations in regions that undergo conformational changes are found to decrease activation energy, accelerate kinetics, and decrease ligand binding affinity (Fields and Somero 1998; Fields et al. 2015). These compensatory changes are likely essential for the continued function of these enzymes in cold temperatures. Our results suggest that, analogous to cold adaptation in enzymes, a similar phenomenon occurs in Antarctic icefish rhodopsins: positively selected mutations occur in regions that undergo light-induced conformational changes, which then decreases ligand (i.e., retinal) binding affinity and activation energy of conformational changes, thereby accelerating return to the dark-state conformation required for recovery of photosensitivity (Schafer and Farrens 2015; Frederiksen et al. 2016; Schafer et al. 2016). This likely accounts for why these sites are under positive selection in cold-adapted icefishes, where cold-induced decreases in kinetic rates would be expected to slow retinal release, thereby delaying dark adaptation and the regaining of photosensitivity (Lamb and Pugh 2006). These compensatory mutations are found in no other vertebrate rhodopsin proteins to our knowledge, which may be due to the negative effects of these mutations on the conformational stability of light-activated rhodopsin under less extreme temperatures. This is consistent with the functional and clinical relevance of light-activated rhodopsin stability, where human disease-associated mutations tend to decrease light-activated rhodopsin stability

**Table 7.** Arrhenius Plot Data for WT, T160A, and I259M Retinal Release.

| Background[a] | Temperature (ln [$K$[b]]) | Rate of Retinal Release (ln [k][c]) |
|---|---|---|
| WT | 3.663004 | −10.4714 |
| | | −9.66711 |
| | | −9.80816 |
| T160A | | −9.93740 |
| | | −9.66486 |
| | | −9.69197 |
| I259M | | −9.54226 |
| | | −9.59076 |
| | | −9.27936 |
| WT | 3.533569 | −8.46052 |
| T160A | | −8.30738 |
| I259M | | −8.37747 |
| WT | 3.412969 | −7.22023 |
| | | −7.18675 |
| | | −7.32077 |
| T160A | | −7.08625 |
| | | −7.00403 |
| | | −7.12042 |
| I259M | | −7.15413 |
| | | −7.10206 |
| | | −7.12878 |

[a]Data were collected from WT bovine (*B. taurus*) rhodopsin, or T160A or I259M mutants.
[b]Natural logarithm of temperature of retinal release assay given in degrees kelvin.
[c]Natural logarithm of rate constants of retinal release assays calculated from fluorescence measurements (Methods), where data were fit to a three variable, first order exponential equation ($y = y0 + a(1 - e^{-bx})$, where $b$ is the rate constant ($k$).

**Table 8.** Multiple Regression Analysis of WT and T160A Retinal Release.

| | Coefficients | Standard Error | t Stat | P-value[a] | Lower 95% | Upper 95% | Lower 95.0% | Upper 95.0% |
|---|---|---|---|---|---|---|---|---|
| Intercept | 29.86088 | 1.644343 | 18.15976 | 1.5E−09 | 26.2417 | 33.48005 | 26.2417 | 33.48005 |
| Temp[b] | −10.8701 | 0.464354 | −23.4092 | 9.82E−11 | −11.8922 | −9.84811 | −11.8922 | −9.84811 |
| Background[c] | 0.188945 | 0.107501 | 1.757609 | 0.106571 | −0.04766 | 0.425555 | −0.04766 | 0.425555 |

[a]P-values shown for a two-sided test.
[b]Retinal release assays were run at 20, 10, and 0 °C.
[c]Data were collected from either WT bovine (*B. taurus*) rhodopsin or T160A mutant.

**Table 9.** Multiple Regression Analysis of WT and I259M Retinal Release.

| | Coefficients | Standard Error | t Stat | P-value[a] | Lower 95% | Upper 95% | Lower 95.0% | Upper 95.0% |
|---|---|---|---|---|---|---|---|---|
| Intercept | 27.35766 | 1.872802 | 14.60788 | 1.51E−08 | 23.23565 | 31.47967 | 23.23565 | 31.47967 |
| Temperature[b] | −10.1625 | 0.52887 | −19.2155 | 8.21E−10 | −11.3265 | −8.99846 | −11.3265 | −8.99846 |
| Background[c] | 0.280017 | 0.122437 | 2.287022 | 0.043002 | 0.010534 | 0.549499 | 0.010534 | 0.549499 |

[a]P-values shown for a two-sided test.
[b]Retinal release assays were run at 20, 10, and 0 °C.
[c]Data were collected from either WT bovine (*B. taurus*) rhodopsin or I259M mutant.

(Stojanovic et al. 2003). It is important to note that we used bovine rhodopsin as a model, rather than icefish rhodopsin. Although our modeling analysis suggests it is unlikely, it remains possible that these mutations may have a different effect within the native icefish rhodopsin background. This would be an interesting subject of future study.

In homeotherms, rhodopsin kinetics are normally accelerated by site-specific interactions with ω-3 polyunsaturated fatty acids such as docosahexaenoic acid (DHA), which is required for optimizing the efficiency of phototransduction and normal rod photosensitivity (Mitchell et al. 2001; Niu et al. 2004; Grossfield et al. 2006; Soubias et al. 2006; Senapati et al. 2018). Unlike homeotherms, however, poikilotherms must alter membrane cholesterol and polyunsaturated fatty acid composition to compensate for the biophysical effects of cold-induced ordering of cell membranes (Logue et al. 2000; Zehmer and Hazel 2005; Ronges et al. 2012), suggesting that fish rhodopsins may be further destabilized by putative increases in the ω-3 polyunsaturated fatty acids such as DHA, which could play a mechanistic role in rhodopsin cold adaptation, where dark-state regeneration is likely slowed by cold temperatures and increased DHA may compensate via accelerated MII decay (Sanchez-Martin et al. 2013). This raises the possibility that in these icefishes, which have some of the highest neural tissue unsaturation levels among vertebrates (Logue et al. 2000), variation at DHA interaction sites may potentially modulate rhodopsin stability in response to variable degrees of membrane lipid unsaturation. Interestingly, M259, which we find to decrease the activation energy required for the return of the dark state, is a site predicted to preferentially interact with DHA (Grossfield et al. 2006) raising the possibility that this site may also play an additional role in rhodopsin cold adaptation through interactions with unsaturated fatty acids that modulate their effects on rhodopsin kinetic and conformational stability, and would be an interesting topic of further investigation.

Despite the ubiquity of membrane lipid adaptations in poikilotherms (Logue et al. 2000; Murray et al. 2007), it is clear that cold adaptation in icefishes is multifaceted, consisting of cascading changes that take place within and across multiple levels of biological organization (Eastman 1993; Beers and Jayasundara 2015). It is also increasingly clear that lipid saturation levels alone do not drive cold adaptation in poikilotherms (Murray et al. 2007; O'Brien and Mueller 2010) and that protein-level changes are integral to organismal temperature adaptation, where a general trend of protein-cold adaptation via mutations decreasing protein activation energy and ligand binding affinity has been repeatedly demonstrated across the tree of life (Siddiqui and Cavicchioli 2006; Portner et al. 2007; Fields et al. 2015; Peck 2016). The location of our mutations, the rare amino acid variants at these key sites, and the functional convergence of rhodopsin consistent with cold adaptation, all point to a role of intrinsic rhodopsin conformational stability in the adaptation of the visual system to extreme cold.

## Evidence for Spectral Tuning in Icefish Rhodopsin

In addition to the novel mutations modifying rhodopsin kinetics, we also identified several spectral tuning residues in icefish that may reflect selective pressure to shift spectral sensitivity of the pigment in response to variable lighting environments. These results highlight the dual constraints exerted on rhodopsin: the protein may be tuned simultaneously with respect to both activation kinetics (e.g., in response to cold) and spectral sensitivity (e.g., in response to changing depths or ambient lighting conditions). For example, one of the kinetics-altering mutations (T160A) modifies the spectral tuning of rhodopsin (red shifts the pigment) in addition to accelerating retinal release rate. This pleiotropic role for site 160 may account for why this mutation switches from A to S across the icefish radiation: in some instances its role in tuning the pigment for spectral content (e.g., to deeper, blue-shifted waters) may be more crucial than cold adaptation, especially since cold adaptation can be achieved through other mutations that do not have pleiotropic effects on spectral tuning (Castiglione et al. 2017, 2018). This is consistent with the variability of amino acid identities at site 83 and 122 across Cryonotothenioids; previous experimental work has revealed a significant role for these sites in both spectral tuning and kinetic adaptation (Breikers et al. 2001; Sugawara et al. 2010; Bickelmann et al. 2012; Dungan and Chang 2017; Hauser et al. 2017; Yue et al. 2017; Castiglione and Chang 2018; Van Nynatten et al. 2021). In sum, Antarctic icefish rhodopsin shows remarkable variability in sites linked to both spectral and kinetic tuning, suggesting that both novel spectral environments (e.g., water columns covered by a layer of ice) as well as cold temperatures have worked in concert to shape rhodopsin function and visual system performance.

## Multiple Molecular Pathways to Convergent Rhodopsin Cold Adaptation Across Fishes

Icefish radiations are thought to arise from a combination of key innovations (e.g., the evolution of AFGPs) and climatic changes creating ecological opportunity (Janko et al. 2007; Barnes and Souster 2011; Matschiner et al. 2011; Near et al. 2012; Colombo et al. 2015; Kasparova et al. 2015; Barnes et al. 2016), where these phenomena in combination drive diversification across lineages (Rutschmann et al. 2011; Eastman 2017). The key icefish mutations we identify and assay (S160A and V259M) occur at two critical time periods wherein major ecological changes (e.g., glaciation and cooling) were driving the rapid radiation of icefish (Near et al. 2012; Colombo et al. 2015; Eastman 2017). Our functional results suggest that icefish rhodopsin proteins exhibit analogous functional properties with cold-adapted rhodopsin previously examined in high-altitude catfishes (Castiglione et al. 2017, 2018); however, unlike spectral tuning adaptations which often occur via the same amino acid substitutions at the same sites (Hunt et al. 2001; Yokoyama et al. 2008), the icefish achieve these nonspectral, kinetic adaptations through different (nonparallel) amino acid

substitutions occurring at different sites. This is highly similar to previous studies, where even in relatively closely-related lineages such as high-altitude Andean and Himalayan catfishes, different mutations to different sites appear to underlie accelerated MII decay rates (Castiglione et al. 2017, 2018). Similar to the convergent high-altitude ecological pressures exerted on these catfishes, there is evidence for convergent diversification in response to parallel ecological pressures in icefish lineages (Rutschmann et al. 2011; Eastman 2017). This functional convergence via nonparallel mechanisms has also been demonstrated in other icefish proteins such as AFGP, where Antarctic fishes have evolved a version from a different precursor than their Arctic counterparts, such as the Arctic cod (Chen et al. 1997). Similarly, cold-adapted $A_4$-LDH enzymes from the same geographic grouping of Antarctic icefishes display functional convergence via nonparallel amino acid substitutions (Fields and Somero 1998). Consistent with this, we could not identify the RH1 mutations studied here in other fishes living in extreme cold conditions (e.g., Arctic cod). The prevalence of nonparallel mutations across instances of functional convergence illustrates how evolution can determine "workarounds" and uncover multiple pathways to adaptation.

## Conclusion

This study is the first to demonstrate cold adaptation in icefish rhodopsin at both molecular evolutionary and functional levels. We found several unique amino acid substitutions in icefish rhodopsin that occur in concert with major physiological and ecological shifts in icefish evolutionary history. These mutations, when experimentally tested, shifted rhodopsin kinetic properties in a manner consistent with cold adaptation, and one of these mutations also resulted in a spectral shift in the protein. Using a combination of molecular evolutionary analyses and protein functional experiments, we have uncovered novel mechanisms of cold adaptation in the visual systems of extremophile icefishes and add to a growing body of work investigating novel, naturally occurring adaptations to extreme cold in signaling proteins.

## Materials and Methods

### Dataset Assembly

Rhodopsin-coding sequences (rh1) originating from Icefishes and outgroups (supplementary tables S1 and S2, Supplementary Material online) were obtained from GenBank. Notothenioid outgroup rh1 sequences were sampled from appropriate phylogenetic orders denoted in Betancur et al. (2013). Rh1 alignments were generated using PRANK codon alignment (Loytynoja and Goldman 2008). The final rh1 alignment encoded for rhodopsin amino acid residues 54–286 (bovine RH1 numbering), inclusively. This encompassed almost the entirety of the

7-transmembrane domain of rhodopsin. We used this alignment to estimate the icefish (Notothenioidei) rh1 gene tree (PhyML) with aLRT branch support (Guindon et al. 2010; supplementary fig. S1, Supplementary Material online). The resulting tree recapitulated all major clades and relationships described in previous species trees (Rutschmann et al. 2011; Near et al. 2012, 2015; Colombo et al. 2015; Hedges et al. 2015; Betancur et al. 2017; Rabosky et al. 2018). Using this alignment and gene tree, we constructed three separate rh1 data sets for phylogenetic analysis: (1) Notothenioids with outgroups (n = 74; supplementary table S1, Supplementary Material online); (2) Notothenioidei (n = 65; supplementary table S1, Supplementary Material online); (3) Cryonotothenioidei (n = 61; supplementary table S1, Supplementary Material online).

### Molecular Evolutionary Analyses

We used codon models of molecular evolution from the PAML 4.7 software package (Yang 2007) to identify evidence of positive selection and accelerated evolutionary rates in rhodopsin-coding sequences (rh1). First, we estimated the evolutionary rates (dN/dS) within each rh1 data set (Notothenioids with outgroups; Notothenioid; Cryonotothenioid) using the random sites models (M1, M2, M3, M7, M8, M8a) implemented in the CODEML program. Next we employed PAML Clade models (Bielawski and Yang 2004) to explicitly test for long-term shifts in evolutionary rates (dN/dS) between foreground and background branches or clades within the rhodopsin data sets. In any partitioning scheme, all nonforeground data are present in the background partition. M2aREL was used as the null model (Weadick and Chang 2012). For all PAML models, multiple runs with different starting priors were carried out to check for the convergence of parameter estimates. Significant differences in model fits were determined by likelihood ratio tests.

### Ancestral Reconstruction

To reconstruct the evolutionary history of sites 160 and 259 we used the Notothenioids with outgroup rh1 alignment and phylogeny described above. This data set was then used to implement codon-based marginal ancestral sequence reconstructions using the PAML 4.7 software package (Yang 2007). Ancestral sequences were chosen from the best-fitting random sites model, which was M8 (table 1, Δ AIC). The likelihood-based reconstruction uses branch lengths and relative substitution rates between nucleotides, followed by empirical Bayesian reconstruction of ancestral codon states at ancestral nodes, where uncertainty is measured as posterior probabilities (Yang et al. 2005; Yang 2006). To identify ancestral codons at the ancestral nodes, we consulted the full posterior probability distribution from the marginal reconstruction, where the character with the highest posterior probability is the best reconstruction (Yang 2006). We verified the absence of T160A and I259M mutations

in noncryonothenioid animal rhodopsins by reference to a Vertebrate RH1 amino acid alignment we assembled using a wide phylogenetic sampling of publicly available *rh1* sequences described previously (supplementary table S2, Supplementary Material online; Castiglione and Chang 2018).

## Rhodopsin Mutagenesis, Expression and Spectroscopic Assays

The complete coding sequence of bovine (*B. taurus*) rhodopsin in the pJET1.2 cloning vector (Thermo Fisher Scientific), as described in a previous study was used here (Castiglione and Chang 2018). Site-directed mutagenesis primers were designed to induce single amino acid substitutions via PCR (QuickChange II; Agilent). All sequences were verified using a 3730 DNA Analyzer (Applied Biosystems) at the Centre for Analysis of Genome Evolution and Function (CAGEF) at the University of Toronto. WT and mutant rhodopsin sequences were transferred to the pIRES-hrGFP II expression vector (Stratagene) for subsequent transient transfection of HEK293T cells (8 μg per 10 cm plate) using Lipofectamine 2000 (Invitrogen). Media was changed after 24 h, and cells were harvested 48 h post-transfection. Cells were washed twice with harvesting buffer (PBS, 10 μg/ml aprotinin, 10 μg/ml leupeptin), and rhodopsins were regenerated for 2 h in the dark with 5 μM 11-*cis*-retinal generously provided by Dr Rosalie Crouch (Medical University of South Carolina). After regeneration the samples were incubated at 4 °C in solubilization buffer (50 mM Tris pH 6.8, 100 mM NaCl, 1 mM CaCl$_2$, 1% dodecylmaltoside, 0.1 mM PMSF) for 2 h and immunoaffinity purified overnight using the 1D4 monoclonal antibody coupled to the UltraLink Hydrazide Resin (Thermo Fisher Scientific). Resin was washed three times with wash buffer 1 (50 mM Tris pH 7.0, 100 mM NaCl, 0.1% dodecylmaltoside) and twice using wash buffer 2 (50 mM sodium phosphate, 0.1% dodecylmaltoside; pH 7.0). Rhodopsins were eluted from the UltraLink resin using 5 mg/ml of a 1D4 peptide, consisting of the last 9 amino acids of bovine rhodopsin (TETSQVAPA).

The UV-visible absorption spectra of purified rhodopsin samples were recorded in the dark at 25 °C using a Cary 4000 double-beam absorbance spectrophotometer (Agilent). All $\lambda_{MAX}$ values were determined by fitting dark spectra to a standard template curve for A1 visual pigments (Govardovskii et al. 2000). Rhodopsin samples were light-activated for 30 s using a fiber optic lamp (Dolan-Jenner), resulting in a shift in $\lambda_{MAX}$ to ~380 nm, characteristic of the biologically active metarhodopsin II intermediate (Van Eps et al. 2017).

Retinal release following rhodopsin photoactivation was monitored using a Cary Eclipse fluorescence spectrophotometer equipped with a Xenon flash lamp (Agilent), according to a protocol modified from previous studies (Farrens and Khorana 1995; Schafer et al. 2016). Rhodopsin samples (0.1–0.2 μM) were bleached for 30 s at 20, 10, or 0 °C with a fiber optic lamp (Dolan-Jenner) using a filter to restrict wavelengths of light below 475 nm to minimize heat. Fluorescence measurements were recorded at 30-s intervals with a 2-s integration time, using an excitation wavelength of 295 nm (1.5 nm slit width) and an emission wavelength of 330 nm (10 nm slit width). There was no noticeable activation by the excitation beam prior to rhodopsin activation. This assay detected increasing fluorescence as a result of decreased quenching of intrinsic tryptophan fluorescence at W265 by the retinal chromophore (Farrens and Khorana 1995), and is a reliable proxy for the tracking the decay of MII (Schafer et al. 2016). Data were fit to a three variable, first order exponential equation ($y = y_0 + a(1 - e^{-bx})$), and half-life values were calculated using the rate constant $b$ ($t_{1/2} = \ln2/b$). All curve fitting resulted in $r^2$ values >0.95. Differences in retinal release half-life values were statistically assessed using a two-tailed *t*-test with unequal variance. Data for Arrhenius plots were collected at 20, 10, and 0 °C. The data were plotted with the reciprocal of the temperature on the *x*-axis, and the natural logarithm of the retinal release on the *y*-axis. A linear regression line was fitted to the data and the slope of the line was used to calculate the activation energy (Ea) based on the Arrhenius equation ($k = Ae^{-Ea/(RT)}$). To determine if rare icefish amino acid substitutions (T160A and I259M) significantly affected the activation energy of retinal release, a multiple linear regression analysis was conducted on retinal release rates derived from different assay temperatures and mutational backgrounds. Effects of independent variables (assay temperature, mutational background) on retinal release rate were considered significant if $P < 0.05$.

## Homology Modeling of Icefish Rhodopsin

To better understand the potential for background protein differences between bovine and icefishes to impact our functional analyses, the structure of icefish RH1 (*C. hamatus*) was computationally estimated from the 3D structure of bovine MII (PDB code: 3PQR; Choe et al. 2011). A 3D structure of icefish MII with all-trans retinal bound was inferred via homology modeling by MODELLER (Sali and Blundell 1993). Minimizing the MODELLER objective function generated 100 separate models, and the run with the lowest discrete optimized protein energy score was assessed (Shen and Sali 2006), with reference to the next four best-fitting models serving as validation of structural changes. For each estimated structure, ProCheck was used to verify the high probability of bond angle and length stereochemical conformations, as indicated by positive overall G-factor (Laskowski et al. 1993). Comparisons of each model's total energy to that expected by random chance were examined using ProSA-web (Wiederstein and Sippl 2007).

## Supplementary Material

Supplementary data are available at *Molecular Biology and Evolution* online.

## Acknowledgments

## Data Availability

The data underlying this article are available in the article and in its online supplementary material.

## References

Aho AC, Donner K, Hydén C, Larsen LO, Reuter T. 1988. Low retinal noise in animals with low body temperature allows high visual sensitivity. *Nature* **334**:348–350.

Barnes DKA, Sands CJ, Hogg OT, Robinson BJO, Downey RV, Smith JA. 2016. Biodiversity signature of the last glacial maximum at South Georgia, Southern Ocean. *J Biogeogr*. **43**: 2391–2399.

Barnes DKA, Souster T. 2011. Reduced survival of Antarctic benthos linked to climate-induced iceberg scouring. *Nat Clim Change*. **1**: 365–368.

Beers JM, Jayasundara N. 2015. Antarctic notothenioid fish: what are the future consequences of 'losses' and 'gains' acquired during long-term evolution at cold and stable temperatures? *J Exp Biol*. **218**:1834–1845.

Betancur RR, Broughton RE, Wiley EO, Carpenter K, López JA, Li C, Holcroft NI, Arcila D, Sanciangco M, Cureton Ii JC, *et al.* 2013. The tree of life and a new classification of bony fishes. *PLoS Curr*. **5**.

Betancur RR, Wiley EO, Arratia G, Acero A, Bailly N, Miya M, Lecointre G, Ortí G. 2017. Phylogenetic classification of bony fishes. *BMC Evol Biol*. **17**:162.

Bickelmann C, Morrow JM, Muller J, Chang BS. 2012. Functional characterization of the rod visual pigment of the echidna (*Tachyglossus aculeatus*), a basal mammal. *Vis Neurosci*. **29**:211–217.

Bielawski JP, Yang Z. 2004. A maximum likelihood method for detecting functional divergence at individual codon sites, with application to gene family evolution. *J Mol Evol*. **59**:121–132.

Breikers G, Bovee-Geurts PH, DeCaluwé GL, DeGrip WJ. 2001. A structural role for Asp83 in the photoactivation of rhodopsin. *Biol Chem*. **382**:1263–1270.

Buckley RG, Trodahl HJ. 1987. Scattering and absorption of visible light by sea ice. *Nature* **326**:867–869.

Castiglione GM, Chang BS. 2018. Functional trade-offs and environmental variation shaped ancient trajectories in the evolution of dim-light vision. *Elife* **7**:e35957

Castiglione GM, Hauser FE, Liao BS, Lujan NK, Van Nynatten A, Morrow JM, Schott RK, Bhattacharyya N, Dungan SZ, Chang BSW. 2017. Evolution of nonspectral rhodopsin function at high altitudes. *Proc Natl Acad Sci U S A*. **114**:7385–7390.

Castiglione GM, Schott RK, Hauser FE, Chang BSW. 2018. Convergent selection pressures drive the evolution of rhodopsin kinetics at high altitudes via nonparallel mechanisms. *Evolution* **72**: 170–186.

Chen L, DeVries AL, Cheng CH. 1997. Convergent evolution of antifreeze glycoproteins in Antarctic notothenioid fish and Arctic cod. *Proc Natl Acad Sci U S A*. **94**:3817–3822.

Cheng CH, Chen L. 1999. Evolution of an antifreeze glycoprotein. *Nature* **401**:443–444.

Choe HW, Kim YJ, Park JH, Morizumi T, Pai EF, Krauss N, Hofmann KP, Scheerer P, Ernst OP. 2011. Crystal structure of metarhodopsin II. *Nature* **471**:651–655.

Cocca E, Ratnayake-Lecamwasam M, Parker SK, Camardella L, Ciaramella M, di Prisco G, Detrich HW III. 1995. Genomic remnants of alpha-globin genes in the hemoglobinless antarctic icefishes. *Proc Natl Acad Sci U S A*. **92**:1817–1821.

Colombo M, Damerau M, Hanel R, Salzburger W, Matschiner M. 2015. Diversity and disparity through time in the adaptive radiation of Antarctic notothenioid fishes. *J Evol Biol*. **28**:376–394.

Crockett EL, Sidell BD. 1990. Some pathways of energy metabolism are cold adapted in Antarctic fishes. *Physiol Zool*. **63**:472–488.

Denton EJ. 1990. Light and vision at depths greater than 200 metres. In: Herring PJ, Campbell AK, Whitfield M, Maddock L, editors. *Light and life in the sea*. Cambridge: Cambridge University Press. p. 127–148.

Dungan SZ, Chang BS. 2017. Epistatic interactions influence terrestrial-marine functional shifts in cetacean rhodopsin. *Proc Biol Sci*. **284**(1850):20162743.

Dungan SZ, Kosyakov A, Chang BS. 2016. Spectral tuning of killer whale (*Orcinus orca*) rhodopsin: evidence for positive selection and functional adaptation in a cetacean visual pigment. *Mol Biol Evol*. **33**:323–336.

Eastman JT. 1988. Ocular morphology in antarctic notothenioid fishes. *J Morphol*. **196**:283–306.

Eastman JT. 1993. *Antarctic fish biology: evolution in a unique environment*. Cambridge, MA: Academic Press.

Eastman JT. 2017. Bathymetric distributions of notothenioid fishes. *Polar Biol*. **40**:2077–2095.

Ebrey T, Koutalos Y. 2001. Vertebrate photoreceptors. *Prog Retin Eye Res*. **20**:49–94.

Ernst OP, Lodowski DT, Elstner M, Hegemann P, Brown LS, Kandori H. 2014. Microbial and animal rhodopsins: structures, functions, and molecular mechanisms. *Chem Rev*. **114**:126–163.

Farrens DL, Khorana HG. 1995. Structure and function in rhodopsin. Measurement of the rate of metarhodopsin II decay by fluorescence spectroscopy. *J Biol Chem*. **270**:5073–5076.

Fields PA, Dong Y, Meng X, Somero GN. 2015. Adaptations of protein structure and function to temperature: there is more than one way to 'skin a cat'. *J Exp Biol*. **218**:1801–1811.

Fields PA, Somero GN. 1998. Hot spots in cold adaptation: localized increases in conformational flexibility in lactate dehydrogenase A4 orthologs of Antarctic notothenioid fishes. *Proc Natl Acad Sci U S A*. **95**:11476–11481.

Frederiksen R, Nymark S, Kolesnikov AV, Berry JD, Adler LT, Koutalos Y, Kefalov VJ, Cornwall MC. 2016. Rhodopsin kinase and arrestin binding control the decay of photoactivated rhodopsin and dark adaptation of mouse rods. *J Gen Physiol*. **148**:1–11.

Govardovskii VI, Fyhrquist N, Reuter T, Kuzmin DG, Donner K. 2000. In search of the visual pigment template. *Vis Neurosci*. **17**:509–528.

Grossfield A, Feller SE, Pitman MC. 2006. A role for direct interactions in the modulation of rhodopsin by omega-3 polyunsaturated lipids. *Proc Natl Acad Sci U S A*. **103**:4888–4893.

Guindon S, Dufayard JF, Lefort V, Anisimova M, Hordijk W, Gascuel O. 2010. New algorithms and methods to estimate maximum-likelihood phylogenies: assessing the performance of PhyML 3.0. *Syst Biol*. **59**:307–321.

Guo Y, Sekharan S, Liu J, Batista VS, Tully JC, Yan EC. 2014. Unusual kinetics of thermal decay of dim-light photoreceptors in vertebrate vision. *Proc Natl Acad Sci U S A*. **111**:10438–10443.

Hauser FE, Chang BS. 2017. Insights into visual pigment adaptation and diversity from model ecological and evolutionary systems. *Curr Opin Genet Dev*. **47**:110–120.

Hauser FE, Ilves KL, Schott RK, Castiglione GM, Lopez-Fernandez H, Chang BSW. 2017. Accelerated evolution and functional divergence of the dim light visual pigment accompanies cichlid colonization of Central America. *Mol Biol Evol.* **34**:2650–2664.

Hedges SB, Marin J, Suleski M, Paymer M, Kumar S. 2015. Tree of life reveals clock-like speciation and diversification. *Mol Biol Evol.* **32**: 835–845.

Hofmann GE, Buckley BA, Airaksinen S, Keen JE, Somero GN. 2000. Heat-shock protein expression is absent in the Antarctic fish *Trematomus bernacchii* (family Nototheniidae). *J Exp Biol.* **203**: 2331–2339.

Hofmann GE, Lund SG, Place SP, Whitmer AC. 2005. Some like it hot, some like it cold: the heat shock response is found in New Zealand but not Antarctic notothenioid fishes. *J Exp Mar Biol Ecol.* **316**:79–89.

Hunt DM, Dulai KS, Partridge JC, Cottrill P, Bowmaker JK. 2001. The molecular basis for spectral tuning of rod visual pigments in deep-sea fish. *J Exp Biol.* **204**:3333–3344.

Imai H, Kuwayama S, Onishi A, Morizumi T, Chisaka O, Shichida Y. 2005. Molecular properties of rod and cone visual pigments from purified chicken cone pigments to mouse rhodopsin in situ. *Photochem Photobiol Sci.* **4**:667–674.

Janko K, Lecointre G, Devries A, Couloux A, Cruaud C, Marshall C. 2007. Did glacial advances during the Pleistocene influence differently the demographic histories of benthic and pelagic Antarctic shelf fishes? –Inferences from intraspecific mitochondrial and nuclear DNA sequence diversity. *BMC Evol Biol.* **7**:220.

Kasparova E, Van de Putte AP, Marshall C, Janko K. 2015. Lifestyle and ice: the relationship between ecological specialization and response to pleistocene climate change. *PLoS One.* **10**:e0138766.

Kawall H, Torres J, Sidell B, Somero G. 2002. Metabolic cold adaptation in Antarctic fishes: evidence from enzymatic activities of brain. *Mar Biol.* **140**:279–286.

Kim BM, Amores A, Kang S, Ahn DH, Kim JH, Kim IC, Lee JH, Lee SG, Lee H, Lee J, et al. 2019. Antarctic blackfin icefish genome reveals adaptations to extreme environments. *Nat Ecol Evol.* **3**:469–478.

Kiss AJ, Mirarefi AY, Ramakrishnan S, Zukoski CF, Devries AL, Cheng CH. 2004. Cold-stable eye lens crystallins of the Antarctic nototheniid toothfish *Dissostichus mawsoni* Norman. *J Exp Biol.* **207**:4633–4649.

Kojima K, Imamoto Y, Maeda R, Yamashita T, Shichida Y. 2014. Rod visual pigment optimizes active state to achieve efficient G protein activation as compared with cone visual pigments. *J Biol Chem.* **289**:5061–5073.

Lamb TD, Pugh EN. 2006. Phototransduction, dark adaptation, and rhodopsin regeneration the proctor lecture. *Investig Opthalmol Vis Sci.* **47**(12):5138–5152.

Laskowski RA, Moss DS, Thornton JM. 1993. Main-chain bond lengths and bond angles in protein structures. *J Mol Biol.* **231**: 1049–1067.

Logue JA, de Vries AL, Fodor E, Cossins AR. 2000. Lipid compositional correlates of temperature-adaptive interspecific differences in membrane physical structure. *J Exp Biol.* **203**:2105–2115.

Loytynoja A, Goldman N. 2008. Phylogeny-aware gap placement prevents errors in sequence alignment and evolutionary analysis. *Science* **320**:1632–1635.

Magnoni LJ, Scarlato NA, Patricio Ojeda F, Wöhler OC. 2013. Gluconeogenic pathway does not display metabolic cold adaptation in liver of Antarctic notothenioid fish. *Polar Biol.* **36**: 661–671.

Matschiner M, Hanel R, Salzburger W. 2011. On the origin and trigger of the notothenioid adaptive radiation. *PLoS One.* **6**:e18911.

Meyer-Rochow VB. 1982. The divided eye of the isopod glyptonotus antarcticus: effects of unilateral dark adaptation and temperature elevation. *Proc R Soc London Ser B Biol Sci.* **215**:433–450.

Meyer-Rochow VB, Laughlin SB. 1997. Intracellular recordings from photoreceptors of the Antarctic isopod Glyptonotus antarcticus. 33rd Int. Congr, Physiol. Sci., St Petersburg 1997, p. 071.01.

Meyer-Rochow VB, Klyne MA. 1982. Retinal organization of the eyes of three nototheniid fishes from the Ross Sea (Antarctica). *Gegenbaurs Morphol Jahrb.* **128**:762–777.

Mitchell DC, Niu SL, Litman BJ. 2001. Optimization of receptor-G protein coupling by bilayer lipid composition I: kinetics of rhodopsin-transducin binding. *J Biol Chem.* **276**:42801–42806.

Morita Y, Meyer-Rochow VB, Uchida K. 1997. Absolute and spectral sensitivities of dark- and light-adapted *Pagothenia borchgrevinki*, an Antarctic Nototheniid fish. *Physiol Behav.* **61**:159–163.

Murray P, Hayward SA, Govan GG, Gracey AY, Cossins AR. 2007. An explicit test of the phospholipid saturation hypothesis of acquired cold tolerance in *Caenorhabditis elegans*. *Proc Natl Acad Sci U S A.* **104**:5489–5494.

Near TJ, Dornburg A, Harrington RC, Oliveira C, Pietsch TW, Thacker CE, Satoh TP, Katayama E, Wainwright PC, Eastman JT, et al. 2015. Identification of the notothenioid sister lineage illuminates the biogeographic history of an Antarctic adaptive radiation. *BMC Evol Biol.* **15**:109.

Near TJ, Dornburg A, Kuhn KL, Eastman JT, Pennington JN, Patarnello T, Zane L, Fernandez DA, Jones CD. 2012. Ancient climate change, antifreeze, and the evolutionary diversification of Antarctic fishes. *Proc Natl Acad Sci U S A.* **109**:3434–3439.

Niu SL, Mitchell DC, Lim SY, Wen ZM, Kim HY, Salem N Jr, Litman BJ. 2004. Reduced G protein-coupled signaling efficiency in retinal rod outer segments in response to n-3 fatty acid deficiency. *J Biol Chem.* **279**:31098–31104.

O'Brien KM, Mueller IA. 2010. The unique mitochondrial form and function of Antarctic channichthyid icefishes. *Integr Comp Biol.* **50**:993–1008.

Palczewski K, Kumasaka T, Hori T, Behnke CA, Motoshima H, Fox BA, Le Trong I, Teller DC, Okada T, Stenkamp RE, et al. 2000. Crystal structure of rhodopsin: a G protein-coupled receptor. *Science* **289**:739–745.

Pankhurst NW, Montgomery JC. 1989. Visual function in four Antarctic Nototheniid fishes. *J Exp Biol.* **142**:311–324.

Parker E, Dornburg A, Struthers CD, Jones CD, Near TJ. 2021. Phylogenomic species delimitation dramatically reduces species diversity in an antarctic adaptive radiation. *Syst Biol.* **71**:58–77.

Peck LS. 2016. A cold limit to adaptation in the sea. *Trends Ecol Evol.* **31**:13–26.

Pointer MA, Cheng C-HC, Bowmaker JK, Parry JWL, Soto N, Jeffery G, Cowing JA, Hunt DM. 2005. Adaptations to an extreme environment: retinal organisation and spectral properties of photoreceptors in Antarctic notothenioid fish. *J Exp Biol.* **208**: 2363–2376.

Portner HO, Peck L, Somero G. 2007. Thermal limits and adaptation in marine Antarctic ectotherms: an integrative view. *Philos Trans R Soc Lond B Biol Sci.* **362**:2233–2258.

Rabosky DL, Chang J, Title PO, Cowman PF, Sallan L, Friedman M, Kaschner K, Garilao C, Near TJ, Coll M, et al. 2018. An inverse latitudinal gradient in speciation rate for marine fishes. *Nature* **559**: 392–395.

Rizzello A, Romano A, Kottra G, Acierno R, Storelli C, Verri T, Daniel H, Maffia M. 2013. Protein cold adaptation strategy via a unique seven-amino acid domain in the icefish (*Chionodraco hamatus*) PEPT1 transporter. *Proc Natl Acad Sci U S A.* **110**:7068–7073.

Ronges D, Walsh JP, Sinclair BJ, Stillman JH. 2012. Changes in extreme cold tolerance, membrane composition and cardiac transcriptome during the first day of thermal acclimation in the porcelain crab *Petrolisthes cinctipes*. *J Exp Biol.* **215**:1824–1836.

Rutschmann S, Matschiner M, Damerau M, Muschick M, Lehmann MF, Hanel R, Salzburger W. 2011. Parallel ecological diversification in Antarctic notothenioid fishes as evidence for adaptive radiation. *Mol Ecol.* **20**:4707–4721.

Ruud JT. 1954. Vertebrates without erythrocytes and blood pigment. *Nature* **173**:848–850.

Sakurai K, Onishi A, Imai H, Chisaka O, Ueda Y, Usukura J, Nakatani K, Shichida Y. 2007. Physiological properties of rod photoreceptor cells in green-sensitive cone pigment knock-in mice. *J Gen Physiol.* **130**:21–40.

Sali A, Blundell TL. 1993. Comparative protein modeling by satisfaction of spatial restraints. *J Mol Biol*. **234**:779–815.

Sanchez-Martin MJ, Ramon E, Torrent-Burgues J, Garriga P. 2013. Improved conformational stability of the visual G protein-coupled receptor rhodopsin by specific interaction with docosahexaenoic acid phospholipid. *ChemBioChem*. **14**:639–644.

Schafer CT, Farrens DL. 2015. Conformational selection and equilibrium governs the ability of retinals to bind opsin. *J Biol Chem*. **290**:4304–4318.

Schafer CT, Fay JF, Janz JM, Farrens DL. 2016. Decay of an active GPCR: conformational dynamics govern agonist rebinding and persistence of an active, yet empty, receptor state. *Proc Natl Acad Sci U S A*. **113**:11961–11966.

Senapati S, Gragg M, Samuels IS, Parmar VM, Maeda A, Park PS. 2018. Effect of dietary docosahexaenoic acid on rhodopsin content and packing in photoreceptor cell membranes. *Biochim Biophys Acta Biomembr*. **1860**:1403–1413.

Shen MY, Sali A. 2006. Statistical potential for assessment and prediction of protein structures. *Protein Sci*. **15**:2507–2524.

Siddiqui KS, Cavicchioli R. 2006. Cold-adapted enzymes. *Annu Rev Biochem*. **75**:403–433.

Soubias O, Teague WE, Gawrisch K. 2006. Evidence for specificity in lipid-rhodopsin interactions. *J Biol Chem*. **281**:33233–33241.

Stojanovic A, Hwang I, Khorana HG, Hwa J. 2003. Retinitis pigmentosa rhodopsin mutations L125R and A164V perturb critical interhelical interactions: new insights through compensatory mutations and crystal structure analysis. *J Biol Chem*. **278**:39020–39028.

Sugawara T, Imai H, Nikaido M, Imamoto Y, Okada N. 2010. Vertebrate rhodopsin adaptation to dim light via rapid meta-II intermediate formation. *Mol Biol Evol*. **27**:506–519.

Sullivan CW, Palmisano AC, Kottmeier S, Grossi SM, Moe R. 1983. The influence of light on development and growth of sea-ice microbial communities in McMurdo sound. *Antarct JUS*. **18**:177–179.

Van Eps N, Caro LN, Morizumi T, Kusnetzow AK, Szczepek M, Hofmann KP, Bayburt TH, Sligar SG, Ernst OP, Hubbell WL. 2017. Conformational equilibria of light-activated rhodopsin in nanodiscs. *Proc Natl Acad Sci U S A*. **114**:E3268–E3275.

Van Nynatten A, Bloom D, Chang BS, Lovejoy NR. 2015. Out of the blue: adaptive visual pigment evolution accompanies Amazon invasion. *Biol Lett*. **11**(7):20150349.

Van Nynatten A, Castiglione GM, de A. Gutierrez E, Lovejoy NR, Chang BSW. 2021. Recreated ancestral opsin associated with marine to freshwater croaker invasion reveals kinetic and spectral adaptation. *Mol Biol Evol*. **38**:2076–2087.

Weadick CJ, Chang BS. 2012. An improved likelihood ratio test for detecting site-specific functional divergence among clades of protein-coding genes. *Mol Biol Evol*. **29**:1297–1300.

Wiederstein M, Sippl MJ. 2007. ProSA-web: interactive web service for the recognition of errors in three-dimensional structures of proteins. *Nucleic Acids Res*. **35**:W407–W410.

Yang Z. 2006. *Computational*. Molecular Evolution: Oxford University Press.

Yang Z. 2007. PAML 4: phylogenetic analysis by maximum likelihood. *Mol Biol Evol*. **24**:1586–1591.

Yang Z, Wong WS, Nielsen R. 2005. Bayes empirical bayes inference of amino acid sites under positive selection. *Mol Biol Evol*. **22**: 1107–1118.

Yokoyama S, Tada T, Zhang H, Britt L. 2008. Elucidation of phenotypic adaptations: molecular analyses of dim-light vision proteins in vertebrates. *Proc Natl Acad Sci U S A*. **105**:13480–13485.

Yokoyama S, Zhang H, Radlwimmer FB, Blow NS. 1999. Adaptive evolution of color vision of the Comoran coelacanth (*Latimeria chalumnae*). *Proc Natl Acad Sci U S A*. **96**:6279–6284.

Yue WW, Frederiksen R, Ren X, Luo DG, Yamashita T, Shichida Y, Cornwall MC, Yau KW. 2017. Spontaneous activation of visual pigments in relation to openness/closedness of chromophore-binding pocket. *Elife* **6**:e18492.

Zehmer JK, Hazel JR. 2005. Thermally induced changes in lipid composition of raft and non-raft regions of hepatocyte plasma membranes of rainbow trout. *J Exp Biol*. **208**:4283–4290.